Eur. Phys. J. B **6**, 399–409 (1998)

THE EUROPEAN PHYSICAL JOURNAL B

Quantum scattering in the strip: From ballistic to localized regimes

R. Gębarowski[1,a], P. Šeba[2,3], K. Życzkowski[4,b], and J. Zakrzewski[5]

[1] Instytut Fizyki, Politechnika Krakowska im. Tadeusza Kościuszki, ul. Podchorążych 1, 30–084 Kraków, Poland
[2] Nuclear Physics Institute, Czech Academy of Sciences, 250 68 Řež near Prague, Czech Republic
[3] Pedagogical University, Hradec Králové, Czech Republic
[4] Institute for Plasma Research, University of Maryland, College Park, MD 20742, USA
[5] Instytut Fizyki im. Mariana Smoluchowskiego, Uniwersytet Jagielloński, ul. Reymonta 4, 30-059 Kraków, Poland

Received: 28 January 1998 / Revised: 16 June 1998 / Accepted: 6 July 1998

Abstract. Quantum scattering is studied in a system consisting of randomly distributed point scatterers in the strip. The model is continuous yet exactly solvable. Varying the number of scatterers (the sample length) we investigate a transition between the ballistic and the localized regimes. By considering the cylinder geometry and introducing the magnetic flux we are able to study time reversal symmetry breaking in the system. Both macroscopic (conductance) and microscopic (eigenphases distribution, statistics of S-matrix elements) characteristics of the system are examined.

PACS. 72.20.Dp General theory, scattering mechanisms – 05.45.+b Theory and models of chaotic systems – 72.10.Bg General formulation of transport theory

1 Introduction

A rapid technological progress in producing small semiconductor and metallic samples, which have the size of the electron phase coherence length, has stimulated extensive investigations of transport through disordered mesoscopic systems [1,2]. Disorder in mesoscopic nanostructures, like for example quantum wires, can be induced by adding some impurities, which serve as electron scatterers and hence modify the electron transport properties. The sample length L and the elastic mean free path, l_e are important parameters for classification of various possible regimes of scattering. In a sample, which size L is of the order of l_e (the ballistic regime), the traveling electron encounters only a few scattering events on its path. However, for samples much longer than the mean free path, the multiple scattering becomes increasingly important. In addition to that, the number of degrees of freedom in the system and the energy of the incoming electron also determine the transmission properties.

Anderson localization is probably the most important phenomenon relevant for such studies [3]. Its generality became fully appreciated after the formulation of the scaling theory [4]. In particular, this theory predicts that extended states (which may lead to the metallic, quantum diffusive regime) are possible only for three-dimensional (3D) and weakly disordered systems, while in one- (1D) or two-dimensional (2D) systems the states are exponentially localized (in the absence of external fields). Special topical meetings devoted to the Anderson localization [5] have covered both theoretical aspects and experimental manifestations of that phenomenon.

A considerable progress has been recently made in understanding transport properties in disordered samples on grounds of the Random Matrix Theory (RMT) [6] (for a recent review see [7]). Moreover, the RMT approach has been successful in explaining statistical properties of fluctuations occurring in the regime of parameters where the corresponding classical scattering exhibits chaos in the interaction region (the so-called chaotic scattering) [8–11]. More general ensembles of random matrices were used to describe quantum systems in the localized regime [12]. In such systems classically chaotic motion corresponds to the disorder in mesoscopic nanostructures.

Not only were the transport phenomena related to electrons under experimental and theoretical scrutiny. A great deal of effort by theorists and experimentalists has been devoted to the electromagnetic wave transport through microwave cavities and guides [8,10,13,14]. Let us

[a] *Present address*: Department of Applied Mathematics and Theoretical Physics, The Queen's University of Belfast, Belfast BT7 1NN, Northern Ireland.
e-mail: `robert@jaguar.am.qub.ac.uk`
[b] Fulbright Fellow.
Permanent address: Instytut Fizyki im. Mariana Smoluchowskiego, Uniwersytet Jagielloński, ul. Reymonta 4, 30-059 Kraków, Poland.

mention that the Anderson localization has been also observed for light scattered in a random medium [15].

So far, numerical studies of a transition from the ballistic to the localized regime have been mainly restricted to tight-binding models. As typical examples one may consider [16,17] for the 1D case, [18] for the 2D model or [19] for 3D calculations. Nevertheless, such models may be regarded as discrete approximations to a continuous scattering problem. While fully appreciating all the results obtained within these approximate models, it is desirable to compare them with those coming from exactly solvable systems (if such are available). In this paper we shall consider such an exactly solvable system, namely a two dimensional strip with N randomly distributed point scatterers. The system has been recently introduced in [20], where it has been shown that, the S-matrix eigenphases obey the Wigner near neighbour statistics for a particular choice of parameters. The aim of present paper is to show a more detailed study of that model, which reveals a smooth transition from the ballistic to localized regime as a number of scatterers (or the sample length) is varied. We investigate both the macroscopic (conductance G) and the microscopic properties of the system (statistical properties of the S-matrix).

It is known for a long time that in the 2D case a proper quantum diffusive regime does not exist typically [4]. However we show that in the transition regime, which is beyond the ballistic regime and yet far from the localized one, the system exhibits similar properties to those expected when the multiple scattering occurs. Thus we are able to observe some resemblance to the behaviour which is typical for the quantum diffusive regime. Let us mention here that this finding is in full agreement with earlier studies [16–18].

The 2D strip model is relevant in description of the disordered transport when the time reversal symmetry is conserved. However this symmetry can be easily destroyed by introducing a magnetic field into the system. In order to demonstrate the capability of our model, we show also that by a change of the geometry and considering a cylinder with the axial magnetic field, it is possible to extend our solvable approach so as to be able to investigate the influence of the magnetic flux inside the cylinder on the scattering occurring on its surface.

The paper is organized as follows. Section 2 gives an overview of the both versions of the model: with and without the magnetic field. In this section we define important physical parameters characterizing the scattering system. The conductance within the model is studied in Section 3, whereas the S-matrix properties are presented in Section 4. Finally, the last section brings the summary and conclusions.

2 The scattering model

A disordered mesoscopic sample is modeled by a 2D hard-wall strip with a finite number N of point scatterers [20]. The geometry of the strip (the scattering region) is described by its length L, which can be varied, and its width which is set at the value $W = \pi$ (results for an arbitrary W may be obtained by a simple rescaling [20]). The point-like scatterers are randomly and uniformly distributed inside the strip with positions $\mathbf{x}_j = (x_j, y_j) \in (-L/2, L/2) \times (0, \pi)$, for $j = 1, ..., N$ (as shown in Fig. 1a).

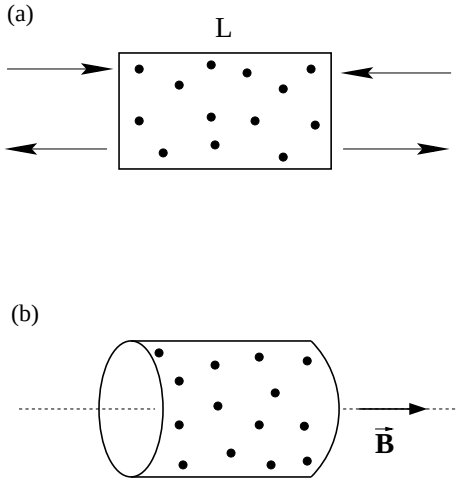

Fig. 1. Schematic diagrams of both models analyzed throughout the paper. (a) Represents the time reversal model consisting of N point scatterers randomly distributed over the strip of width π and length L. (b) Shows a cylinder of the perimeter 2π with N point scatterers on its surface. The magnetic flux inside the cylinder breaks the time reversal invariance.

It is assumed that the scattering in the strip is elastic and the wavefunction vanishes on the horizontal strip boundaries (hard walls) so that

$$\psi(x, 0) = \psi(x, W) = 0, \qquad \text{for all } x. \tag{1}$$

Appropriate boundary conditions [20] are also set on small circles of radius a_j surrounding the jth point scatterer. Everywhere except the inside of the circles the Hamiltonian of the system corresponds to the free propagation, $H_0 = -\Delta$ (in the units $\hbar/(2m) = 1$). Together with the boundary conditions mentioned above this procedure allows for a rigorous construction of a self-adjoint extension of the Hamiltonian in the presence of singular point perturbers. We refer the mathematically oriented reader to [20] for details of this particular model, while the extensive discussion of mathematical techniques used to solve singular point interaction problems may be found in [21]. For the purpose of the present study, it suffices to say that the real parameters α_j characterizing the self adjoint extension are related to a_j by $\alpha_j = -\ln(a_j)/2\pi$ [22]. In the following we shall take these perturbers to be identical by setting $\alpha_j = \alpha$ for all j. A large positive value of α corresponds to a weak perturbation, and in particular the perturbation can be removed by taking a limit $\alpha \to \infty$ so that the self adjoint extension is simply equal to H_0.

The number of channels M in which the electron may enter the system from either side of the strip is equal to the integer part of the length of the total wave-vector $\mathbf{k}$ of the incoming electron. Let a^l_{in} and a^r_{in} denote the M-component vectors representing the waves incoming

from the left and the right side of the strip, respectively (depicted in Fig. 1a as the two arrows pointing towards the strip from left and right). The outgoing waves from the left and right side of the strip (shown in Fig. 1a by the two arrows pointing outwards) are described by a^l_{out} and a^r_{out}, respectively. The scattering process can be described by a $2M \times 2M$ unitary matrix S. The S-matrix relates amplitudes of the incoming waves with those which represent outgoing ones so that $\{a^l_{out}, a^r_{out}\} = S\{a^l_{in}, a^r_{in}\}$ and therefore it has the following block structure

$$S = \begin{pmatrix} r & t \\ t' & r' \end{pmatrix}, \tag{2}$$

where r and r' are reflection matrices whereas t, t' are transmission sub-blocks, each of them having size $M \times M$.

The advantage of the model with singular point-like perturbers is that explicit formulae for the S-matrix elements are available [20]

$$r_{nm}(E) = \frac{i}{\sqrt{2\pi}} \sum_{j,k=1}^{N} [\Lambda(E)^{-1}]_{jk} \frac{\sin(my_j)\sin(ny_k)}{\sqrt{k_m(E)k_n(E)}} \times \exp[i(k_m x_j + k_n x_k)] \tag{3}$$

and

$$t_{nm}(E) = \delta_{n,m} + \frac{i}{\sqrt{2\pi}} \sum_{j,k=1}^{N} [\Lambda(E)^{-1}]_{jk} \frac{\sin(my_j)\sin(ny_k)}{\sqrt{k_m(E)k_n(E)}} \times \exp[-i(k_m x_j - k_n x_k)], \tag{4}$$

where E is the energy of incident electrons. The $N \times N$ matrix $\Lambda(E)$ is given by its elements

$$\Lambda_{jj}(E) = \alpha + \frac{1}{\pi} \sum_{n=1}^{\infty} \left[\frac{1}{2n} - \frac{i \sin^2(ny_j)}{k_n(E)} \right], \tag{5}$$

and

$$\Lambda_{jm}(E) = -\frac{i}{\pi} \sum_{n=1}^{\infty} \frac{\exp(ik_n(E)|x_j - x_m|)}{k_n(E)} \times \sin(ny_j)\sin(ny_m), \qquad j \neq m. \tag{6}$$

The longitudinal momentum k_n satisfies the relation

$$k^2 = k_n^2 + n^2, \tag{7}$$

hence for $n > k$, it becomes imaginary ($k_n \sim in$), what ensures the convergence of the series (5).

Conductance in the strip can be calculated using the famous Landauer formula

$$G = G_0 \sum_{n,m=1}^{M} \mathrm{Tr}\{tt^\dagger\}, \tag{8}$$

where $G_0 = e^2/h$ (we omit the spin degeneracy factor). Since the matrix S is unitary, $\mathrm{Tr}\{tt^\dagger\} = \mathrm{Tr}\{t't'^\dagger\} = M - \mathrm{Tr}\{rr^\dagger\}$, so the transmission (reflection) coefficients for electrons entering the strip from both sides are equal. In the following we work in dimensionless units and omit the proportionality factor G_0.

In order to break the time reversal symmetry we introduce a magnetic field into the model [20]. It is convenient to modify the strip with scatterers into a cylinder of length L and perimeter 2π, as shown in Figure 1b. Periodic boundary conditions read now

$$\psi(x,0) = \exp\left(i\frac{\Phi_B}{2\pi}\right)\psi(x,2\pi)$$
$$\frac{\partial}{\partial y}\psi(x,0) = \exp\left(i\frac{\Phi_B}{2\pi}\right)\frac{\partial}{\partial y}\psi(x,2\pi), \tag{9}$$

where Φ_B is the magnetic flux inside the cylinder. Since the cylinder can be mapped onto the rectangle $\Omega = [0, L] \times [0, 2\pi)$, the solutions obtained in the case of the strip can be modified accordingly – for more details see [20]. The longitudinal momentum depends in this case on the magnetic flux, so equation (7) has to be replaced by the following

$$k_n(E) = \sqrt{E - (n + \Phi_B/(2\pi))^2}, \qquad n = 0, \pm 1, ..., \pm M. \tag{10}$$

Let us point out that both versions of the model are continuous and exactly solvable in the sense that the scattering matrix elements can be written analytically (albeit in terms of infinite series). We believe therefore that this makes the model extremely interesting and useful for investigating the statistical properties of S-matrices and for analysis of conductance in disordered mesoscopic media.

In order to get a proper statistical sample of data we average the studied properties over several realizations of random positions of N scattering points for both versions of the model (the strip and the cylinder with the magnetic flux). We choose the local density of the scattering points, ρ, to be constant by setting $L = N$ (this choice yields the scatterers density $\rho = 1/\pi$ for the strip and twice as smaller value for the cylinder model). Hence throughout this paper we shall use the sample length L to parameterize the model. We consider the perturbers to be strong and take $\alpha = 0$ (recall that $\alpha \to \infty$ corresponds to a vanishing perturbation).

As it has been pointed out in the introduction, the elastic mean free path l_e is yet another important parameter which determines the regime of the scattering behaviour. It is therefore crucial to establish its value for the discussed model. The total cross-section σ for the scattering on a single point-like impurity in 2D may be obtained from an appropriate formula valid for the scattering in the plane [21] and for $\alpha = 0$ it reads

$$\sigma = \frac{\pi^2}{k} \frac{1}{[\gamma + \ln(k/2)]^2 + \pi^2/4}, \tag{11}$$

where $\gamma \approx 0.577...$ is the Euler constant. The mean free path itself can be expressed in terms of the total cross section and the density of point-like impurities $l_e = 1/\rho\sigma$. Note that, because the density ρ is constant as a result

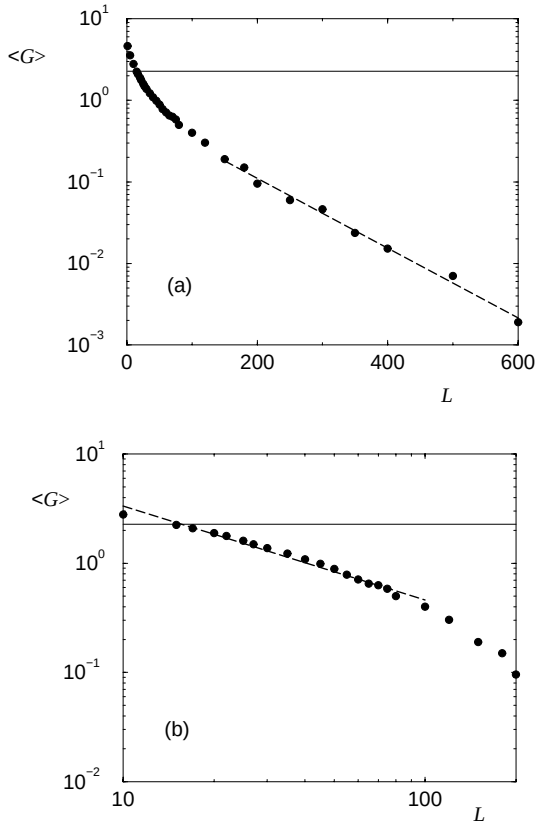

Fig. 2. (a) The mean conductance $\langle G\rangle$ as a function of the length of the strip L (the number of point scatterers $N = L$) for $M = 5$ open channels. The numerical data, each representing an average over 400 realizations are represented by filled circles. For a sufficiently long sample the exponential decay of $\langle G\rangle$ with L is observed. The dashed line yields the fit of the localization length $\xi = 100 \pm 3$. Thin horizontal line shows, for a reference, $\langle G\rangle_R = 2.27$ value assuming that S pertains to the COE. (b) Shows a part of the data in the transition between the ballistic and the localized regimes. Observe that a power-law dependence of $\langle G\rangle$ on L quite well approximates the behaviour of the mean conductance in this region. The horizontal straight line represents the RMT value, the same as in (a).

of the choice $N = L$, the mean free path has a fixed value for a given incident energy (or the value k of the wavevector). This allows for approaching various regimes of the scattering simply by changing the length of the strip together with the number of the randomly distributed impurities.

3 Conductance of the strip

To achieve the ballistic (or quasi-ballistic) regime, the sample length L (equal, in our model to the number of point like scatterers N) should be of the order of the elastic mean free path l_e. The latter strongly depends on the wavevector k (the integer part of which gives the number of open channels M) – compare equation (11). In most of the discussed numerical examples we shall take $k = 5.5708$, which corresponds to $M = 5$. This yields $l_e \approx 8.9$ for the strip model.

Once we have that $N \gg l_e$, the multiple scattering in the sample becomes possible. Incoming waves are strongly distorted in this regime. Since quantum diffusion does not appear in 2D [4] we expect a smooth transition from the ballistic to the localized regime for a sufficiently large $L = N$.

The Λ matrix elements are given by infinite sums, compare equations (5, 6). For realistic computation times (all calculations have been performed on a personal computer) we have to restrict the analysis to moderate L values. For that reason we have chosen $M = 5$ in most of our numerical studies.

Figure 2a shows on the logarithmic scale the dependence of the mean conductance $\langle G\rangle$ on the length of the strip L. Observe that for $L \geq 100$, the conductance decays exponentially with L as expected for sufficiently long samples in the localization regime. A fit to the exponential decay of the mean conductance, $\langle G\rangle \propto \exp(-L/\xi)$ (shown in the figure with a broken line), yields an estimate for the localization length $\xi = 100 \pm 3$. The mean conductance for shorter samples is presented in Figure 2b in the double logarithmic scale. Note that for values $L \in (10, 100)$, a straight line well approximates the data, thus yielding the power-low dependence on the sample size L, $\langle G\rangle \propto L^{-c}$ with $c = 0.90 \pm 0.05$. This is not, however, an indication of the quantum diffusive regime (where according to the theory $\langle G\rangle$ should be proportional to L^{-1}), but it rather stems from the fact that the sample is shorter than the localization length ξ. Thus the localization (depending on the quantum interference occurring on the length scale of ξ) cannot fully set in. Therefore, what we really observe here is a transition from the ballistic regime (dominated by direct processes) to a fully localized situation.

The introduction of point perturbers into a classically integrable system leads to a seemingly "quantum chaotic" behaviour for a finite value of $\hbar$ – the so-called wave chaos [23,24]. Hence, it is interesting to compare the behaviour of our model with point scatterers with that predicted for chaotic scattering models. For the sake of such analysis, it has been conjectured that the Random Matrix Theory [6] approach correctly captures the statistical properties of the S-matrix [8,10] (for the equilibrated component – using the nuclear physics language [25], or after unfolding the S-matrix – see next section – using the language typical for RMT applications to bound systems). On the ground of this conjecture statistical properties of the unitary matrix S may be represented by random matrices of Dyson circular ensembles [26].

Leaving a more detailed microscopic comparison for the next section, let us consider here the mean conductance and its variance. For the S-matrix pertaining to the Circular Orthogonal Ensemble (COE), which is relevant for the strip model preserving the time-reversal symmetry, the RMT yields a value for the mean conductance (including the weak localization correction) and its variance [7,10] which may be expressed in terms of the number

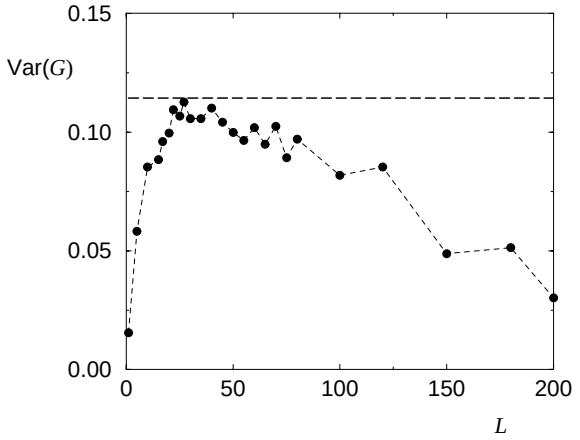

Fig. 3. The variance of the conductance distribution for the same parameters as in Figure 2. The dashed line corresponds to the RMT prediction (see text). Note that in the transition region Var(G) remains close to the RMT value and is only weakly dependent on L.

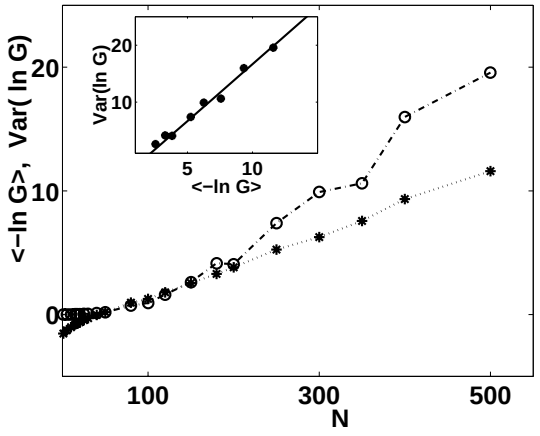

Fig. 4. The mean logarithmic conductance $\langle \ln G \rangle$ (asterisks) and its variance $\mathrm{Var}_{\ln}$ (open circles) as a function of the strip length L for $M = 5$ open channels. The inset shows the dependence of the variance on the mean – the theoretical prediction for the localized regime is depicted with the line. For more discussion see text.

of channels M as follows

$$\langle G \rangle_R = \frac{M}{2} - \frac{M}{4M+2}, \tag{12}$$

$$\mathrm{Var}_R(G) = \frac{M(M+1)^2}{(2M+1)^2(2M+3)}\,. \tag{13}$$

The above formulae yield $\langle G \rangle_R = 2.27$ and $\mathrm{Var}_R(G) = 0.1144$, when the number of channels $M = 5$ is taken.

Observe that while the mean conductance rapidly passes through the RMT value (depicted with a horizontal solid line in both panels of Fig. 2), the behaviour of the variance is markedly different (compare Figs. 2b and 3 – in the latter the value of $\mathrm{Var}_R(G)$ is depicted by a dashed horizontal line). The variance rapidly increases when L exceeds the value corresponding to the mean free path l_e, then saturates in the vicinity of the RMT value and afterwards again rapidly falls down for $L > \xi$. Thus in the "transition" region defined by the interval $l_e < L < \xi$, a rapid, almost linear change on the logarithmic scale in $\langle G \rangle$ is accompanied by a relatively weak dependence of the Var(G) on L – a phenomenon closely resembling universal conductance fluctuations in metallic samples.

In our case the direct processes strongly influence $\langle G \rangle$. Intuitively, in the transition region they should affect the variance to a lesser extent. In this region the localization does not set fully yet (since the sample is too short) and we observe the multiple scattering (typical for a chaotic process) which manifests itself in the value of the variance being close to the RMT prediction. We mention, however, that for the problem studied we are not in the semiclassical regime since the number of open channels is too small as well as the singular perturbers do not have a proper classical limit (that is in such a limit, their perturbing effect disappears completely).

In the localization regime, the conductance becomes vanishingly small, it is therefore much more informative to study not the conductance itself but its logarithm. In Figure 4 both the mean logarithmic conductance $\langle -\ln G \rangle$ (asterisks) and its variance (circles) are presented. For a strip length taken from the interval $L \in (25, 100)$ (the transition region) both the mean and the variance of the logarithmic conductance take approximately the same values. On the other hand, for $L > 200$ there is a clear growth of the variance $\mathrm{Var}_{\ln} = \langle [\ln G - \langle \ln G \rangle]^2 \rangle$ which satisfies in this range of L values the relation

$$\mathrm{Var}_{\ln} = 2\langle -\ln G \rangle \tag{14}$$

predicted for localized regime [7,19,27,28] as shown in the inset with a solid line. In fact, the linear regression fit for the numerical data yields the slightly smaller value 1.90 ± 0.09 for the slope.

Not only the mean conductance and its variance but also the distribution of the conductance may be studied. According to the predictions of the RMT [7,19], in the quantum diffusive regime the distribution of the conductance, $P(G)$, is a Gaussian for a large number of channels $M \gg 1$. Nevertheless, some results for the transport through chaotic cavities [10] indicate that already for $M = 3$ the conductance distribution appears to be approximately a Gaussian. We observe a similar behaviour in the transition region (between the ballistic and localized regimes) discussed above. Exemplary data for such a case are displayed in Figure 5a, where the conductance distribution is shown for $L = 20$ (it has been obtained from 10^4 configurations of random scatterers). In the figure a thin solid line shows a Gaussian distribution with the mean and its variance calculated from that statistical representation. Thus not only the variance but the whole distribution of the conductance in the transition region behaves in the way associated typically with the metallic regime.

The distribution $P(G)$ changes with an increase of the number of the scatterers (and the length of the strip)

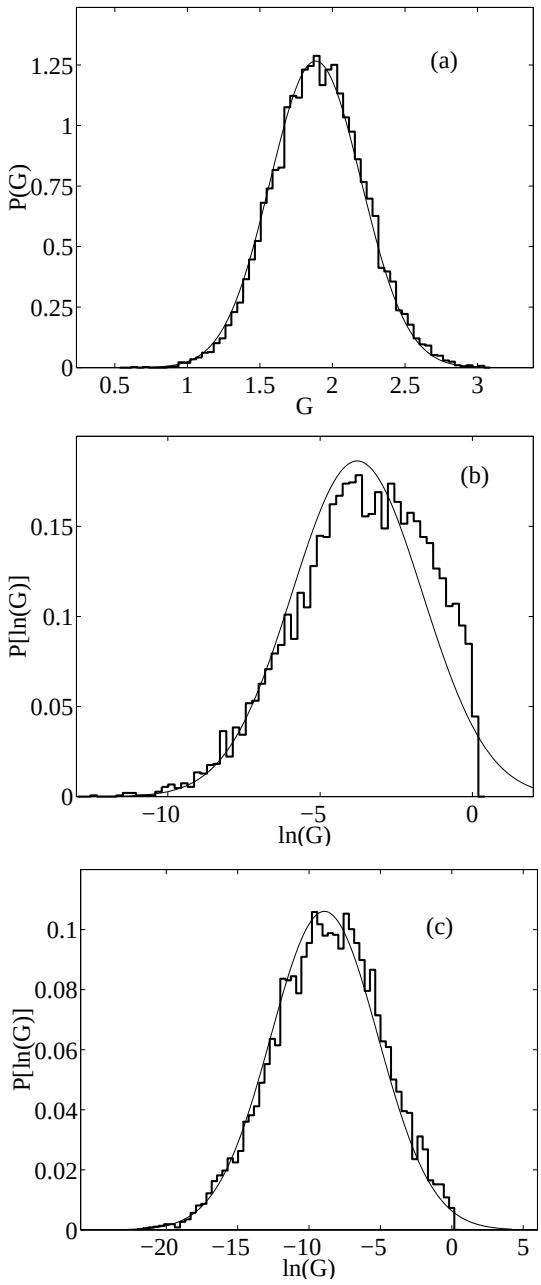

Fig. 5. Conductance distributions, $P(G)$, obtained for $M = 5$ and for the length of the sample (strip) L equal to (a) 20, (b) 200 and (c) 400 ($N = L$ in each case as usual). Data in (a) are drawn in the linear scale and are compared to the normal distribution. Data in (b) and (c) obtained for the localized regime are displayed as $P(\ln G)$, while the thin solid line in both panels represents theoretically predicted log-norm distribution for the localized regime.

and once it reaches the localized regime, it can be approximated by a log-normal distribution [7,19,29]

$$P(\ln G) = \frac{1}{\sqrt{2\pi\sigma_{\ln}^2}} \exp\left[- \frac{(\ln G - \langle \ln G \rangle)^2}{2\sigma_{\ln}^2} \right] \qquad (15)$$

with the mean and variance related to each other by equation (14). The distribution (15) of the logarithmic conductance is due to the nature of the localization, where the total wavefunction can be super-imposed of partial wavefunctions, which have very small overlaps. Thus, the total transmission probability is given by a product of component transmissions, which explains the origin of a Gaussian distribution of logarithms of the conductance.

In Figure 5 – panels (b) and (c) – we present the distribution of the logarithmic conductance for $L = 200$ and $L = 400$, respectively. Let us mention that the log-normal distribution (15) (depicted in both panels by a thin solid line) well describes the conductance fluctuations only in the latter case. Although in Figure 2 we have seen clearly the indications of the localization occurring for $L > 100$, it fully sets in for much longer samples for which additionally the logarithmic conductance obeys closely the log-normal distribution.

Let us partially summarize the results obtained directly from the studies of measurable quantity – the conductance of the strip. For short samples, $L \approx l_e$, the scattering is dominated by direct processes – the ballistic scattering occurs. For long samples the mean conductance decreases exponentially with L yielding the localization length $\xi \approx 100$ (for $M = 5$ case studied). The relatively broad transition region $l_e < L < \xi$ exhibits a behaviour reminiscent of the quantum diffusion in 3D metallic samples: an approximately linear decrease of the mean conductance $\langle G \rangle$ with the inverse sample size L^{-1} (the Ohm law, a similar behaviour for a tight binding 1D model has been reported in [16]), the variance is roughly independent of the mean conductance (an analog of the universal conductance fluctuations), and finally the conductance has a Gaussian distribution. It is interesting to see whether the microscopic properties (S-matrix elements, its eigenphases) likewise support that description of the scattering regimes.

4 Microscopic properties

The most well-known tool in studies of statistical properties of a sample of levels is the nearest neighbour spacing distribution [6,30]. For an ensemble of unitary S-matrices, the corresponding measure is the distribution of eigenphase spacings (*i.e.* writing the eigenvalues as $\exp(i\theta_j)$ we consider the distances $\theta_{j+1} - \theta_j$ for $j = 1, ..., (2M-1)$, for a $2M \times 2M$ scattering matrix). For the COE a good approximation for the eigenphases spacing distribution is the Wigner surmise [30]. Such a distribution is expected also for the chaotic scattering occurring in the ballistic regime [8,10], provided that the direct processes are eliminated (*i.e.* the processes which contribute to a non-vanishing average over the ensemble, $\langle S \rangle \neq 0$). In the case of $\langle S \rangle = 0$ one expects an uniform distribution of eigenphases over the interval $[0, 2\pi)$.

When the direct processes are important one should first eliminate their contribution from the S-matrix (*i.e.* "unfold" this matrix) by considering $S_{fl} = S - \langle S \rangle$, where $\langle S \rangle$ is the matrix obtained by an arithmetic mean of S-matrix elements over different realizations of the disorder. Several procedures for "unfolding" the S-matrix have

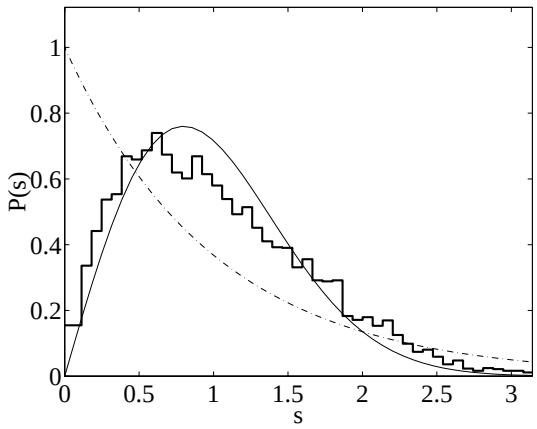

Fig. 6. The spacing distribution $P(s)$ obtained for unfolded eigenphases (see text) of the S-matrix in the situation when direct processes dominate the scattering (the length of the strip $L = 5$ is smaller than the mean free path l_e, the number of open channels $M = 5$). The numerical data shown in the form of a histogram are compared with the Wigner (thin solid line) and the Poisson (dashed line) distribution.

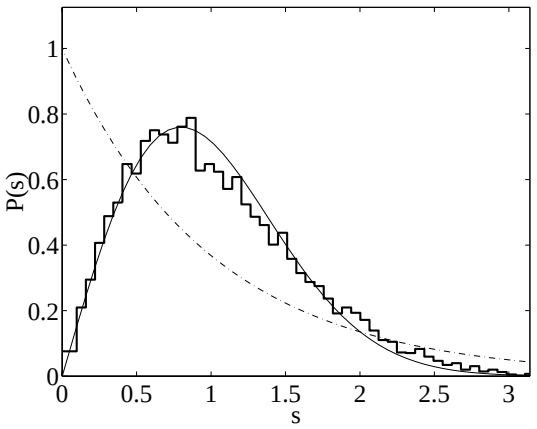

Fig. 7. Same as Figure 6 but data are for $L = 40$, *i.e.*, in the transition region between the ballistic and the localized regime.

been proposed [17,25,31] – we have followed the prescription of Friedman and Mello [31]. Let us mention that in [18] another unfolding procedure, borrowed from studies of bound systems [32] has been used.

Let us consider first an extremely short sample of the length $L = 5$. The resulting spacing distribution $P(s)$ after the unfolding procedure is shown in Figure 6 (a heavy line). It is well-approximated neither by the Poisson (a dashed line) nor the Wigner distribution (a thin solid line), though the latter far better fits to the data than the former one especially for small spacing values s. For $L < l_e$, at most one scattering event perturbs the incoming wavefunction, so there is no reason to expect a good agreement with RMT predictions.

As soon as we enter the transition region ($l_e < L < \xi$, see the previous section), the direct scattering ceases to be the dominant process, and the multiple scattering comes into play. The initial wavefunction becomes strongly distorted while passing through the sample and indeed the spacing distribution is much better approximated by the Wigner distribution (compare Fig. 7 displaying data for $L = 40$). This is consistent with the discussion presented in the previous section (a Gaussian distribution of the conductance, an approximate independence of its variance on L).

As mentioned above, in the transition region, where the multiple scattering is important, a coherent backscattering should appear for the time reversal system due to interference between multiple scattering paths passing in the opposite directions. This effect is a manifestation of the "weak localization" and has been observed in earlier studies, both for electron [5,33] and light waves [15]. In the 3D case it appears for energies above the transition to the localization (when $kl_e > 1$).

A similar effect can be seen when S-matrices are treated within the RMT approach. The mean squared modulus of matrix elements averaged over the COE/CUE ensembles (the latter being the Circular Unitary Ensemble) reads (*e.g.* [7])

$$\langle |S_{mn}|^2 \rangle_\beta = \frac{1 - (1 - 2/\beta)\delta_{mn}}{2\ M - 1 + 2/\beta}, \tag{16}$$

with $\beta = 1$ and 2 for the COE and CUE, respectively. The presence of an enhanced diagonal in this distribution for $m = n$ is a distinct footprint of the time reversal symmetry (see also [34,35]).

In order to test whether the weak localization effect appears in the transition region we turn to the cylinder model since it allows us to perform breaking of the time-reversal symmetry by introducing the magnetic flux (see Sect. 2). In Figure 8 the scattering probabilities $|S_{mn}|^2$, averaged over an ensemble of 10^3 S-matrices (each of them corresponding to a particular configuration of random point scatterers) are presented for the case corresponding to the fixed momentum $k = 10.5708$ and the cylinder length $L = 200$. Since the density of scatterers is $\rho = 1/2\pi$, using (11) we obtain $l_e \approx 50$. Indeed, the enhancement of the backscattering to the same channel is clearly visible in the case of null magnetic flux (see panel (a) – the anti-diagonal of the reflection sub-blocks rather than the diagonal elements are twice as larger than the off-diagonal elements due to the choice of the channel basis representation [20] suitable for the cylinder version of the model). The selective enhancement of the reflection is destroyed as the axial magnetic field is turned on as demonstrated in panel (b), showing results for the magnetic flux $\Phi_B/(2\pi) = 0.1$.

It is worth emphasizing that in Figure 8 there is also visible a clear enhancement on the diagonal of the transmission matrix which is an indication of the presence of direct processes (the data presented are not unfolded). Also the off-diagonal elements of reflection matrices are several times bigger than the transmission matrices elements.

Let us consider now the limiting case of an extreme localization. The incoming wave is fully reflected, that is t, $t' \approx 0$ and the reflection sub-blocks r, r' are unitary (this property of S-matrix was discussed earlier

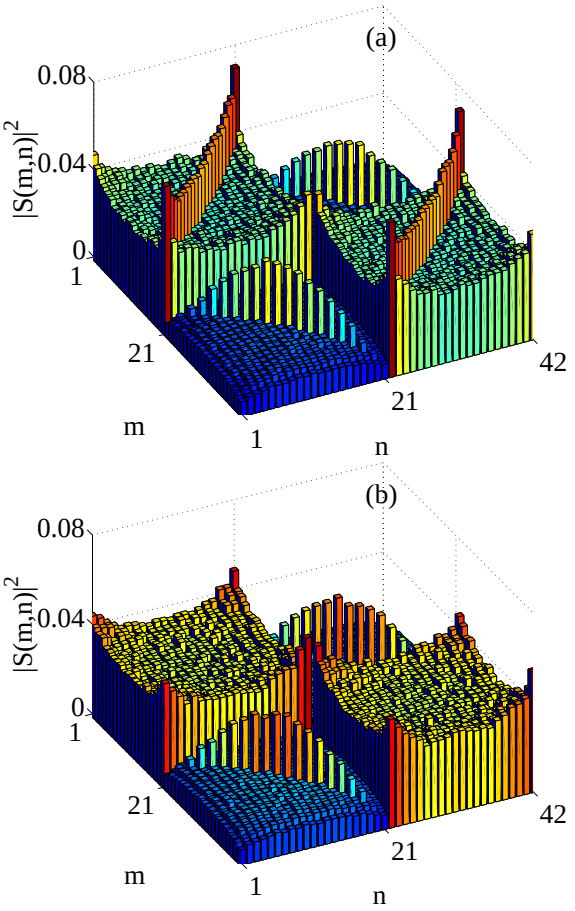

Fig. 8. Scattering probabilities $|S_{mn}|^2$, averaged over 10^3 configurations of random points, for the cylinder model with $k = 10.5708$ and $L = 200$. (a) Shows a 3D diagram for null magnetic flux, $\Phi_B = 0$, while (b) shows data for this system with the magnetic flux $\Phi_b/(2\pi) = 0.1$ inside the cylinder. Note the difference in the diagonal elements corresponding to the reflection blocks (the anti-diagonals rather than the diagonals of sub-matrices r, r' are enhanced due to a specific choice of the channel ordering used in the case of the cylinder – compare [20]). The number of open channels is $M = 21$ in both (a) and (b).

in [17,18]). The reflection is a result of complicated scattering events, hence both matrices r, r' may be considered as those pertaining to the COE (or CUE for the cylinder model with the magnetic field). Actually, as discussed in detail in [18], such a situation occurs for quasi-1D samples only, the transverse dimensions of the sample lead to deviations from RMT predictions. Recall, however, that we consider the strip of width $W = \pi$ and the length $L \gg W$ so indeed we may consider this to be a quasi-1D situation.

The scattering matrix S, equation (2), in the fully localized case, consists thus of two independent diagonal blocks, each pertaining to an appropriate circular ensemble. Therefore spectral properties of the entire S-matrix correspond to a superposition of two independent COE (or CUE) spectra. The level spacing distribution for such a case does not reveal any usual effect of level repulsion but it is rather described by the Berry-Robnik distribution [36] for two disconnected chaotic regions of equal volume. While in [36] the time-reversal invariant situation is mainly discussed, the same formalism is easily extended for unitary ensembles. Approximating the spacing distribution for the COE by the corresponding Wigner distribution (exact, strictly speaking for Gaussian 2×2 matrices only [30]) one easily obtains

$$P_O(s) = \frac{\pi}{8} s \, \exp\left(-\frac{\pi}{16} s^2\right) \operatorname{erfc}\left(\frac{\sqrt{\pi}}{4} s\right) + \frac{1}{2} \exp\left(-\frac{\pi}{8} s^2\right) \quad (17)$$

for the approximate spacing distribution in this case. The standard form, $\operatorname{erfc}(z) = (2/\sqrt{\pi}) \int_z^\infty \exp(-t^2) dt$, for the error function is used above.

Before presenting the numerical data let us point out that the choice of the initial basis leading to the particular form (2) of the scattering matrix is somewhat arbitrary. Taking a different order of components in the vector describing the outgoing wave we may write $\{a^l_{out}, a^r_{out}\} = S'\{a^r_{in}, a^l_{in}\}$ where the scattering matrix S' now has the form

$$S' = \begin{pmatrix} t & r \\ r' & t' \end{pmatrix}. \quad (18)$$

Both forms (2, 18) of the scattering matrix describe the same physical phenomenon. However, in the extreme localization regime (t, $t' \approx 0$) the statistical properties of S and S' are not the same. The matrix S' consists of two off-diagonal unitary blocks r and r'. We show in the Appendix that the eigenvalues of such a matrix are given by

$$\operatorname{eig}(S') = \{\operatorname{eig}(\sqrt{rr'}), -\operatorname{eig}(\sqrt{rr'})\}. \quad (19)$$

If unitary matrices r and r' pertain to the CUE (and are distributed uniformly according to the Haar measure), so does their product rr'. As a result of that, the spectrum of S' consists of two replicas of a CUE-like spectrum, rescaled by the factor of two.

Let us assume that, for the time reversal version of the model, r and r' can be described by the COE. Using a concept of composed unitary ensembles it was shown that in such a case the product rr' fulfills a weaker property. It displays the COE-like spectrum, in spite of the fact, that it does not pertain to the COE [37]. Thus the local statistical properties of S' (analyzed at the scale of mean level spacings $d \ll M$) are the same as those of the corresponding circular ensembles, in contrast to the properties of S.

The spectral properties of S and S' are different also in a realistic case of a nonzero conductance. To demonstrate that we present in Figure 9 numerical results obtained for $L = 800$, *i.e.* far into the localization regime. Panel (a) shows the spacing statistics $P(s)$ for the matrix S whereas panel (b) displays that statistics for the S'-matrix. It is evident that the spacings distributions for S and S' are indeed very much distinct, the former being quite reasonably

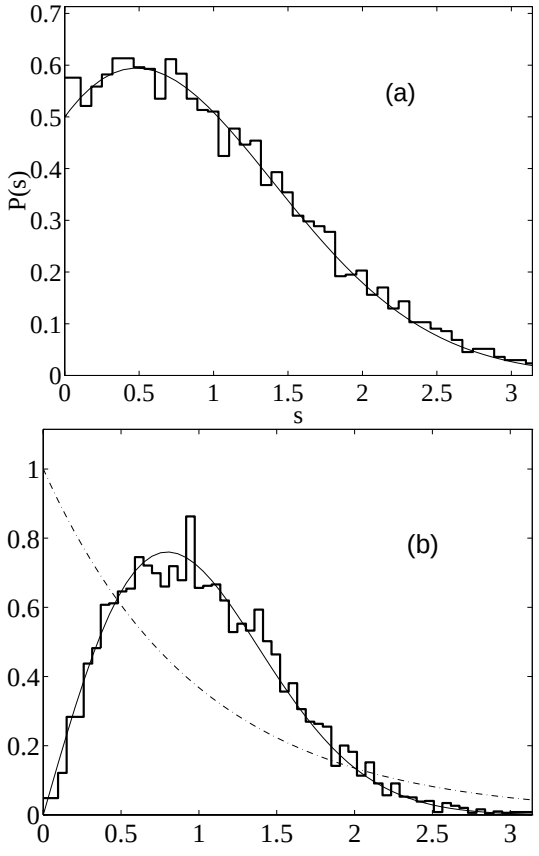

Fig. 9. Comparison of the spacing distribution $P(s)$ for the S-matrix as defined by equation (2) (a) and that for S' defined *via* equation (18) (b) for long samples $L = 800$ and $M = 5$. While the latter is well-approximated by the Wigner distribution (a thin solid line in (b)), the former shows much better agreement with the Berry-Robnik distribution (a thin solid line in (a)) corresponding to a superposition of two independent random ensembles as further discussed in text.

approximated by (17) while the latter by the Wigner distribution (a thin solid line). It has to be emphasized that this supports the conjecture that two uncoupled COE-like matrices may represent both reflection sub-matrices.

This finding is also consistent with tight-binding model calculations [18], where similar agreement has been found for quasi-1D situations. It has been shown in that paper [18] that when "transverse" dynamics becomes important the number variance of S-matrix eigenphases, $\Sigma^2(d)$, exceeds that for two uncoupled COE's. As discussed in [18] only $0 < d \ll M$ range is interesting since all $2M$ eigenphases must fall in $(0, 2\pi)$ interval. Hence, for the discussed numerically case, $M = 5$, we are limited to low values of d only. As shown in Figure 10, in this interval we observe quite nice agreement between $\Sigma^2(d)$ for reflection matrices of the strip model with $L = 800$ (a heavy solid line) and predictions for the COE (a thin solid line). However, for shorter samples, $L = 200$ (a heavy dashed line), where the localization is not fully set as discussed in the previous section, the number variance displays significant deviations from the COE behaviour for $d > 1.5$. Due to a nonzero conductance the reflection matrices r and r' are not unitary, but the statistics of the eigenphases can still be described by random matrices of circular ensemble. This is no longer true for a larger conductance (shorter length L of the strip).

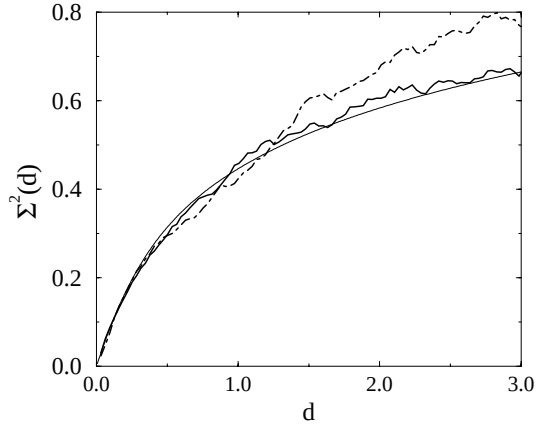

Fig. 10. The number variance, $\Sigma^2(d)$ for the reflection submatrix r in the deep localization regime of the scattering: $L = 800$ and $M = 5$ (a heavy solid line). Note a nice agreement with the COE prediction (a thin solid line). For shorter samples $L = 200$ (a heavy dashed line), the number variance shows disagreement with the COE behaviour for $d > 1.5$.

5 Conclusions

In this paper we have discussed quantum scattering and the transition from the ballistic to the localized regime in the explicitly solvable model of point scatterers in the strip. The model reproduces the Gaussian distribution of the conductance in the diffusive regime and the log-normal distribution when the length of the strip is large enough to reach the localization regime. The number of point scatterers which is necessary for representing the localized regime strongly increases with the momentum of the incident electron (the number of open channels).

We find that the statistics of eigenphases of the S-matrix is of the Wigner type not only, as expected, in the diffusive regime, but provided a specific structure of the S-matrix is taken, it may also reveal the distinctive level repulsion property in the localized regime. This is in contrast to the case of quantized autonomous chaotic systems for which dynamical localization manifest itself by a Poissonian like level statistics [30]. Therefore, our results demonstrate that the spectral properties of the scattering matrix cannot be used as a sole criterion for the localization. On the other hand, the localization in the system manifests itself in the statistical properties of the reflection and transmission submatrices of S.

The results obtained within present model are in full agreement with similar earlier studies [16–18]. However, while those studies were based on tight binding

models (which necessarily discretize continuum) the present model is continuous and yet explicitly solvable.

The model allows one to include also effects due to a magnetic flux and thus to follow a gradual breaking of the time reversal symmetry. It is also possible to introduce a geometric reflection symmetry (for example by drawing randomly the position of $N/2$ scatterers only and taking the remaining half as their mirror image with respect to the symmetry line) and analyze the symmetric case discussed earlier in [38,39]. In addition, the model may be used to analyze other statistical properties such as the distribution of Wigner time-delays [14,40,41] or other parametric properties of the S-matrix.

Finally, we would like to mention that the results of the model discussed in the present paper, may be relevant also for experimental studies. These might include systems like quantum wires doped with a number of impurity atoms, whose configurations can be randomize by a thermal process [42]. In such a system, the conductance and its variance behaviour could be investigated with an increasing number of impurity atoms (and the length of the sample). Another possibility is to carry out measurements in a microwave domain, investigating the propagation through waveguides with antennas [43], where breaking of the time reversal symmetry has been recently realized experimentally for microwave billiards [44]. In addition, an experimental study of microscopic properties of the scattering matrix also could be feasible, for example by looking at the backscattering to the same channel as compared to the reflection to any other channel, in the presence and absence of the time reversal symmetry.

One of us (RG) wishes to acknowledge financial support through the fellowship awarded by the Foundation "Nadace pro podporu teoretické fyziky" from Slemeno near Rychnov nad Kněžnou in the Czech Republic and the hospitality at Instytut Fizyki, Uniwersytet Jagielloński in Kraków. Another of us (KŻ) thanks Ed Ott for hospitality at the Institute for Plasma Research, University of Maryland, where part of this work has been done and acknowledges the Fulbright fellowship. Financial support by Komitet Badań Naukowych and the grant GAAV CR 1048804 is also gratefully acknowledged.

Appendix

Let us consider the following algebraic lemma:

Lemma

Let A and B be $M \times M$ unitary matrices and let C reads

$$C = \begin{pmatrix} 0 & A \\ B & 0 \end{pmatrix}. \tag{A.1}$$

Then the spectrum of C is given by

$$\mathrm{eig}(C) = \{\mathrm{eig}(\sqrt{AB}), -\mathrm{eig}(\sqrt{AB})\}. \tag{A.2}$$

Proof of the lemma

Let eigenvalues and eigenvectors of $\sqrt{AB}$ be denoted by d and U respectively, so that $d = U^\dagger \sqrt{AB} U$. Consider an $2M \times 2M$ matrix X defined as

$$X = \frac{1}{\sqrt{2}} \begin{pmatrix} U & U\sqrt{AB}B^\dagger \\ -U & U\sqrt{AB}B^\dagger \end{pmatrix}. \tag{A.3}$$

It is easy to show that X is unitary. Direct computation allows us to verify that X consists of eigenvectors of C, so that

$$XCX^\dagger = \begin{pmatrix} d & 0 \\ 0 & -d \end{pmatrix}, \tag{A.4}$$

which proves the lemma.

References

1. *Mesoscopic Phenomena in Solids*, edited by B.L. Altshuler, P.A. Lee, R.A. Webb (North Holland, Amsterdam, 1991).
2. E. Akkermans, G. Montambaux, J.L. Pichard, J. Zinn-Justin, Session LXI 1994, *Mesoscopic Quantum Physics*, Editions Les Houches (Elsevier Science B.V., Amsterdam, 1995).
3. P.W. Anderson, Phys. Rev. **109**, 1492 (1958).
4. E. Abrahams, P.W. Anderson, D.C. Licciardello, T.V. Ramakrishnan, Phys. Rev. Lett. **42**, 673 (1979).
5. see *e.g. Anderson Localization, Proc. Int. Symp., Tokyo*, Japan August 16–18, 1987, edited by T. Ando, H. Fukuyama (Springer-Verlag, Berlin, Heidelberg, 1988), and references quoted in the Introduction.
6. M.L. Mehta, *Random Matrices*, 2nd edn (Academic Press, New York, 1991).
7. C.W.J. Beenakker, Rev. Mod. Phys. **69**, 731 (1997).
8. R. Blümel, U. Smilansky, Phys. Rev. Lett. **60**, 477 (1988).
9. U. Smilansky in *Chaos and Quantum Physics*, Les Houches Session LII 1989, edited by M.-J. Giannoni, A. Voros (North-Holland, Amsterdam, 1991).
10. H.U. Baranger, P.A. Mello, Phys. Rev. Lett. **73**, 142 (1994).
11. P.A. Jalabert, J.-L. Pichard, C.W.J. Beenakker, Europhys. Lett. **27**, 255 (1994).
12. K.A. Muttalib, M.E.H. Ismail, J. Phys. A **28**, L451 (1995).
13. H.-J. Stöckmann, J. Stein, Phys. Rev. Lett. **64**, 2215 (1990).
14. Y. Fyodorov, H.-J. Sommers, J. Math. Phys. **38**, 1918 (1997).
15. D.S. Wiersma, P. Bartolini, A. Lagendijk, R. Righini, Nature **390**, 671 (1997).
16. F. Borgonovi, I. Guarneri, J. Phys. A **25**, 3239 (1992).
17. F. Borgonovi, I. Guarneri, Phys. Rev. E **48**, R2347 (1993).
18. P.A. Jalabert, J.-L. Pichard, J. Phys. I France **5**, 287 (1995).
19. K. Slevin, *Electron Transport and Localisation in Disordered Solids*, Proc. QCTM, Fukui (1993), J. Phys. Soc. Jpn **63** Suppl. A, 170 (1994).
20. P. Exner, P. Gawlista, P. Šeba, M. Tater, Ann. Phys. **252**, 133 (1996).

21. S. Albeverio, F. Gesztesy, R. Hoegh-Krohn, H. Holden, *Solvable Models in Quantum Mechanics* (Springer-Verlag, New York, Berlin, Heidelberg, 1988).
22. P. Exner, P. Šeba, Phys. Lett. A **222**, 1 (1996).
23. P. Šeba, Phys. Rev. Lett. **64**, 1855 (1990).
24. P. Exner, P. Šeba, A.F. Sadreev, P. Středa, P. Feher, Phys. Rev. Lett. **80**, 1710 (1998).
25. C.H. Lewenkopf, H.A. Weidenmüller, Phys. Rev. Lett. **68**, 3511 (1992).
26. F.J. Dyson, J. Math. Phys. **3**, 140 (1962).
27. O.N. Dorokhov, Pis'ma Zh. Eksp. Teor. Fiz. **36**, 259 [JETP Lett. **36**, 318] (1982).
28. G. Casati, I. Guarneri, G. Maspero, J. Phys. I France **7**, 729 (1997).
29. Y. Imry, Europhys. Lett. **1**, 249 (1986).
30. F. Haake, *Quantum Signatures of Chaos* (Springer, Berlin, 1991).
31. W.A. Friedman, P.A. Mello, Ann. Phys. **161**, 276 (1985).
32. O. Bohigas, in *Chaos and Quantum Physics*, Les Houches Session LII 1989, edited by M.J. Giannoni, A. Voros (North-Holland, Amsterdam, 1991).
33. G. Bergmann, Phys. Rev. B **25**, 2937 (1982).
34. P.A. Mello, E. Akkermans, B. Shapiro, Phys. Rev. Lett. **61**, 459 (1988).
35. P.A. Mello, A.D. Stone, Phys. Rev. B **44**, 3559 (1991).
36. M.V. Berry, M. Robnik, J. Phys. A **17**, 2413 (1984).
37. M. Poźniak, K. Życzkowski, M. Kuś, J. Phys. A **31**, 1059 (1998).
38. V.A. Gopar, M. Martinez, P.A. Mello, H.U. Baranger, J. Phys. A **29**, 881 (1996).
39. K. Życzkowski, Phys. Rev. E **57**, 2257 (1997).
40. P. Šeba, K. Życzkowski, J. Zakrzewski, Phys. Rev. E **54**, 2438 (1996).
41. V.A. Gopar, P.A. Mello, Europhys. Lett. **42**, 131 (1998).
42. D. Mailly, M. Sanquer, J. Phys. I France **2**, 357 (1992).
43. S. Albeverio, F. Haake, P. Kurasov, M. Kuś, P. Šeba, J. Math. Phys. **37**, 4888 (1996).
44. U. Stoffregen, J. Stein, H.-J. Stöckmann, M. Kuś, F. Haake, Phys. Rev. Lett. **74**, 2666 (1995).